INTERNATIONAL JOURNAL OF HYDROGEN ENERGY 44 (2019) 4897–4906

Available online at www.sciencedirect.com

ScienceDirect

journal homepage: www.elsevier.com/locate/he

Hydrogen adsorption, dissociation, and diffusion on high-index Mg(10$\bar{1}$3) and their comparisons with Mg(0001): A systematic first-principles study

Jia-Hui Ye [a], *Yu-Jun Zhao* [b], *Yan-Xiong Fang* [a], *Huai-Jun Lin* [c], *Lei Bai* [d], *Jia-Jun Tang* [a,b,*]

[a] *School of Chemical Engineering and Light Industry, Guangdong University of Technology, Guangzhou, 510006, China*

[b] *Department of Physics, South China University of Technology, Guangzhou, 510640, PR China*

[c] *Institute of Advanced Wear & Corrosion Resistant and Functional Materials, Jinan University, Guangzhou, 510632, China*

[d] *West Virginia University, Department of Chemical and Biomedical Engineering, Morgantown, 26506, WV, United States*

ARTICLE INFO

Article history:
Received 26 October 2018
Received in revised form
31 December 2018
Accepted 2 January 2019
Available online 28 January 2019

Keywords:
Mg surface
H adsorption
H dissociation
H diffusion
Highindex
First-principles

ABSTRACT

We have systematically studied the hydrogen adsorption mechanism, hydrogen dissociation, and diffusion on the high-index experimentally-found Mg(10$\bar{1}$3) surface and made comparisons with the low-index Mg(0001) surface, using density-functional theory calculations. Various possible H adsorption sites and structures on the high-index Mg(10$\bar{1}$3) are considered with H coverage up to eight monolayers. Specifically, the hydrogen adsorption sequence is found to be A_1-fcc, A_2-fcc, A_1-tetra II, A_2-tetra II, A_3-fcc, B_1-hcp, B_2-hcp and B_1-octa. The H–Mg–H trilayer with $Mg^{1.60+}$ and $H^{0.80-}$ is found to be very stable during initial H uptake, while the H electron gain of 0.8 *e* (i.e., $H^{0.80-}$) is shown to be a reliable indicator of H-adsorbed Mg(10$\bar{1}$3) stability. Interestingly, on the one hand, H_2 dissociation is the role step during H uptake on Mg(10$\bar{1}$3) with an H_2 dissociation energy barrier of 0.87 eV, which is consistent with the value on the low-index Mg(0001) from previous first principle calculations. On the other hand, the H diffusion barriers along the closed-packed planes are lower than those perpendicular to the planes, verifying that more feasible diffusion paths are available on the high-index Mg(10$\bar{1}$3). These theoretical findings rationalize the previous joint experimental finding that the high-index Mg(10$\bar{1}$3) dramatically decreases H sorption temperatures, and provide an H adsorption mechanism on high-index Mg surface very different from that on low-index Mg(0001), thus improving the foundation of Mg-based hydrogen storage material designs.

* *Corresponding author*. School of Chemical Engineering and Light Industry, Guangdong University of Technology, Guangzhou, 510006, China.
E-mail address: pcntsfad@gmail.com (J.-J. Tang).

https://doi.org/10.1016/j.ijhydene.2019.01.012
0360-3199/

Introduction

Seeking a dependable, cost-efficient and flexible energy source has been a long sought-after goal for easing the incongruity between the undesirable climate change partly caused by fossil fuel burning and the energy demand for sustainable development. Hydrogen exhibits a high energy density of 142 MJ/kg, and it represents a green and sustainable substitute for fossil fuels [1–3]. With the advantages of low cost, great abundance and high capacity, Mg and Mg-based alloys have been considered to be one of the most promising hydrogen storage material candidates. Magnesium hydride (MgH_2), with the gravimetric hydrogen capacity of 7.7 wt% as well as the high energy density of 9.9 MJ/kg, has attracted numerous interests. However, the disadvantages including slow sorption rate of hydrogen and the high operating temperature (~575 K) limit practical applications [4–8].

Numerous efforts were aimed at reducing the hydrogen sorption temperature and the kinetic energy barrier. The sorption kinetics at moderate temperature can be enhanced by magnesium composites, which contain light elements or 3*d*-transition metals, and are prepared by high energy ball milling, such as Mg–Ti–Zr, Mg–V, Mg–Mn, Mg–Fe, Mg–Ni, and Mg–Co, MgH_2–$LiNH_2$, Mg–Al [9–13]. Besides, nanostructuring Mg, with an increased surface area, could achieve lower-enthalpy adsorption by storing the formation heat as excess surface energy [14,15]. It is noteworthy that high-index Mg(10$\bar{1}$3) surface has been successfully synthesized where the hydrogen desorption temperature decreased to 392 K [16], lower than MgH_2 formation temperature of 423.15 K [17] and H desorption temperature of 453.15 K achieved by the plasma carbon–modified MgH_2/TiC [18]. In the meanwhile, *ab initio* calculations demonstrate that, on the one hand, hydrogen was more expedient to penetrate into the bulk along the hexagonal close-packed planes of the Mg(10$\bar{1}$3) surface. However, on the other hand, hydrogen penetration through the close-packed plane into the Mg(0001), the conventionally experimentally observed Mg surface, has a high energy barrier. Thus, Mg(10$\bar{1}$3) dramatically improves the H kinetics by providing H penetration with a path along the hexagonal close-packed planes, capable of being a promising hydrogen storage material.

Crystallographic features considerably affect the interface and surface structures, resulting in various sorption properties of different high- and low-index surfaces. For example, the mixture of molecular and dissociative water adsorption is the most stable on UO_2[111]/PuO_2[111] surface, whereas the dissociative water is more energetically favored than the molecular one on UO_2[110]/UO_2[100] and PuO_2[110]/PuO_2[100] surface [19,20]. IrO_2(100) is inactive for CH_4 reactions at a moderate temperature, but IrO_2(110) surface is greatly beneficial to C–H bond cleavage, which remarkably reduces the activation temperature to 150 K [21]. It has been shown that surface structures and relative stabilities of various high- and low-index Mg surfaces can be simply described by the different numbers of basal band non-basal bonds cut on various surfaces [22]. Importantly, the energy difference between cutting basal bonds (i.e., the Mg–Mg bond in the same close-packed plane) and non-basal ones indicates the stronger Mg–Mg basal bonding due to closer in-plane Mg–Mg distance [22]. This theoretical understanding well explains the improved H kinetics of experimentally prepared high-index Mg(10$\bar{1}$3) and rationalizes that low-index surfaces (e.g., Mg (10$\bar{1}$0)) are not necessarily more stable than high-index ones [16]. Moreover, the intriguing sorption and kinetic property difference between low-index Mg(0001) and high-index Mg(10$\bar{1}$3) implies the critical role of high-index Mg surface to hydrogen storage application. For further understanding the working mechanism of high-index surfaces, there is a need for a detailed investigation into H sorption and kinetic properties. Though a clear theoretical picture for the thermodynamics and kinetics of H sorption on high-index Mg(10$\bar{1}$3) has been qualitatively provided [16], there can be more work to be done. The details of hydrogen adsorption, on the one hand, have not been fully provided. For example, the site difference between on-surface sites (i.e. top, bridge, fcc and hcp) and subsurface ones (i.e. octa, tetra I and tetra II) on low-index Mg(0001) [23] has not been discussed on high-index Mg(10$\bar{1}$3) [16], while the details of hydrogen adsorption sequence and charge distribution on Mg and H on H-adsorbed structures during hydrogen uptake are lacking. Additionally, the theories of hydrogen dissociation [24–28], adsorption [23,28–31] and diffusion [24,28,30,32] on Mg(0001) have been well established by Vegge 2004; Du et al., 2006; Pozzo et al., 2008; Pozzo and Alfè 2008, 2009a, 2009b; Li et al., 2009; Jiang et al., 2010; Lei et al., 2013; Xin et al., 2016; Han et al., 2017. The high barrier of H_2 dissociation and the "blocking effect" of H diffusion are two main hinders during H uptake [33]. Furthermore, transition metal-doped Mg(0001) has also been extensively studied, especially the doping of V, Ni, Rh and Co could dramatically decrease the dissociation barrier [28,34–38]. Naturally, the data on Mg(10$\bar{1}$3) are expected. The comparisons between the above-mentioned contents and those of Mg(0001) surface, on the other hand, can be made. We assume that these understandings on H sorption properties are necessary for obtaining solid fundamentals of for further possible improvements on hydrogen sorption properties on high-index Mg surfaces.

In this paper, we systematically investigate the hydrogen adsorption on Mg(10$\bar{1}$3) surface by employing density-functional theory (DFT) calculations. We discuss H adsorption energies and geometries on Mg(10$\bar{1}$3) surface, and then investigate H adsorption mechanism at the specific positions. By inspecting the structures desorption, bonding property, electron distribution and charge allocation, we attempt to figure out an indicator related to the stability of H/Mg(10$\bar{1}$3). Based on H adsorption sequence, H_2 dissociation and H penetration are also studied to determine the step of H uptake. Comparisons between data of Mg(10$\bar{1}$3) and that of Mg(0001) in this paper and pervious literatures provide an explanation for the facilitated H uptake of Mg(10$\bar{1}$3) in our pervious experiment.

Computational method

The first-principles calculations based on the framework of density functional theory (DFT) are performed using the

Vienna *ab initio* simulation package (VASP) with the projector-augmented-wave(PAW) pseudopotentials and generalized-gradient approximation (GGA) [39–42]. The plane-wave energy cutoff is set to be 400 eV for all calculations. For each model, the hexagonal close-packed (hcp) bulk Mg is adopted with the calculated lattice constants of $a = b = 3.190$ Å, $c = 5.17$ Å with the c/a ratio of 1.62 and an included angle of 120° between a and b axes, and a cohesive energy of 1.52 eV/Mg atom, which are well consistent with previous reports [22,28,43] as well as the experimental values ($a = 3.21$ Å, $c/a = 1.62$ and a cohesive energy of 1.51 eV/atom) [44,45].

For hydrogen adsorption on pure Mg(0001) surface, Mg(0001) surface is modeled by a twenty-atom surface in a (2 × 2) supercell with a vacuum layer of 12 Å. Mg(10$\bar{1}$3) surface is fabricated from a (2 × 4) supercell of eleven Mg atomic layers, each of which consists of four Mg atoms, with a vacuum layer of 12 Å. The lattice and Mg atoms of the (2 × 4) Mg(10$\bar{1}$3) model are fully relaxed, and the included angle between lattice vectors are relaxed to be 90°(a and c), 99.3°(a and b) and 90°(b and c). The lowermost two and four layers of Mg atoms are fixed in Mg(0001) and Mg(10$\bar{1}$3), respectively. For simulating the process of hydrogen uptake, the hydrogen atoms are gradually placed on both sides of the outermost Mg layers (i.e., various H coverage, θ, is considered). A (5 × 5 × 1) and a (3 × 3 × 1) Monkhorst-Pack k-point grids are employed for Mg(0001) and Mg(10$\bar{1}$3) surfaces for the integration of Brillouin zone [46]. A (9 × 9 × 1) Monkhorst-Pack grid is used for the models used in Bader Charge analysis, the projected density of states (PDOS) and the charge density analysis. On Mg(10$\bar{1}$3), there are four equivalent adsorption sites at one monolayer. The adsorption coverage (θ) with four equivalent adsorption sites occupied by one, two, three and four hydrogen atoms is deemed to be 0.25, 0.5, 0.75, and 1 monolayer (ML). The force convergence criteria for atom involved is less than 10^{-5} eV between successive ionic steps and the forces are less than 0.001 eV/Å.

To evaluate the structural stability, average adsorption energy (E_{ad}) per hydrogen is calculated by equation (1).

$$E_{ad} = \frac{1}{N_H}\left[E_{MgH} - \left(E_{Mg} + \frac{N_H}{2}E_{H_2}\right)\right], \quad (1)$$

where N_H represents the number of the adsorbed hydrogen atoms in the system, and E_{MgH}, E_{Mg} are the total energies of the Mg–H system and the clean Mg surface in each model, while E_{H_2} is the energy of H_2 in the gas phase. The more negative E_{ad} is, the more exothermic (stable) the structure is.

The H_2 dissociation and H diffusion processes are performed with the Nudged Elastic Band (NEB) method [47]. A 20-atom (2 × 2) Mg(0001) model and 24-atom (2 × 2) Mg(10$\bar{1}$3) model are fabricated. Five images are used in H_2 dissociation and 7 images are adopted in H diffusion to obtain the minimum energy pathway and energy barrier, and the number of images is enough through the tests. The Monkhorst-Pack k-point grids is set to be (4 × 4 × 1) for Mg(0001) and (5 × 3 × 1) for Mg(10$\bar{1}$3), whereas the energies and total forces convergence criteria for all the atoms of images are 1×10^{-4} eV and 0.03 eV/Å.

Results and discussion

H adsorption sequence on Mg(10$\bar{1}$3) surface

The adsorption order of hydrogen atom on Mg(10$\bar{1}$3) surface from 1 to 8 ML are systematically studied layer by layer. There are various adsorption sites, including top, bridge, fcc and hcp, octahedral, tetrahedral hollow sites, which are considered as the potential adsorption sites during the hydrogen uptake. Previous studies have concluded that H located at the bridge or top hollow sites is not energetically favorable on Mg(0001), and adsorption sites on the Mg(10$\bar{1}$3) share similar characteristics [16,23]. Therefore, the fcc (f), hcp (h), tetrahedral I (tetra I), tetrahedral II (tetra II) and octahedral (octa) sites are mainly considered in this section. As shown in Fig. 1a, there are two stacking Mg closed-packed planes, along the [0001] orientation, named Plane A and B, respectively. For adsorption site nomenclature, we distinguish the two types of hollow sites on these two planes as depicted in Fig. 1a) and b), while the subscript number represents the order from the outermost Mg atomic layer to the inner ones along the [10$\bar{1}$3] orientation (viz., notice that the layer on Mg(10$\bar{1}$3) is different from the sliding Plane A and B). For example, Mg (B_3) denotes the third outmost Mg atom on plane B, and H (B_1-tetra I) is hydrogen atom located at the tetrahedral I hollow site of the outmost Mg on Plane B.

Table 1 lists that the A_1-fcc, A_2-hcp, B_1-hcp, B_2-fcc hollow sites are energetically favorable for the first H atoms to be adsorbed. The most stable hydrogen is situated in A_1-fcc hollow site, and the adsorption energy is −0.132 eV, lower than that of hydrogen located at B_1-hcp site by 0.051 eV. Moreover, the adsorption energies used in Section 3.3 are listed in Table 2, which supports that the models are reasonable compared to other reports, as manifested by the favorable adsorption sites as well as the close adsorption energies that are in good convergence. The preferred adsorption sites are studied every single layer, and the adsorption energies are shown in Table S1 ~ S8 and are directly depicted in Fig. 2. The energetically favored adsorption sequence is: A_1-fcc, A_2-fcc, A_1-tetra II, A_2-tetra II, A_3-fcc, B_1-hcp, B_2-hcp and B_1-octa.

H prefers to adsorb at A_1-fcc hollow sites when coverage is less than 1 ML. Furthermore, favorable adsorption sites at 1 ML < θ < 2 ML are studied based on the 1 ML configuration where A_1-fcc sites are fully occupied. It is worthy to note that the H (A_2-fcc) has an overwhelming advantage on adsorption energy, which drops from −0.146 to −0.201 eV/H when the coverage increases from $\theta = 1$ ML to $\theta = 2$ ML. H adsorption energies at the other adsorption sites, including A_2-hcp, B_1-hcp and B_2-fcc A_1-tetra I, A_1-tetra II and A_1-octa hollow sites, are slightly less negative, which means these configurations are not as energetically favored as the H (A_1-fcc)/H (A_2-fcc) configuration.

When 2 ML < θ < 4 ML, the most energetically favorite adsorption sites are A_1-tetra II and A_2-tetra II with the E_{ad} moderately increasing from −0.201 to −0.153 eV/H, indicating that the formation of the "H–Mg–H trilayer" structure is dominating as coverage increases. Afterward, it is more likely for H to adsorb on Plane B, and the hydrogen uptake on Plane B is analogous to that of Plane A: two hydrogen monolayers

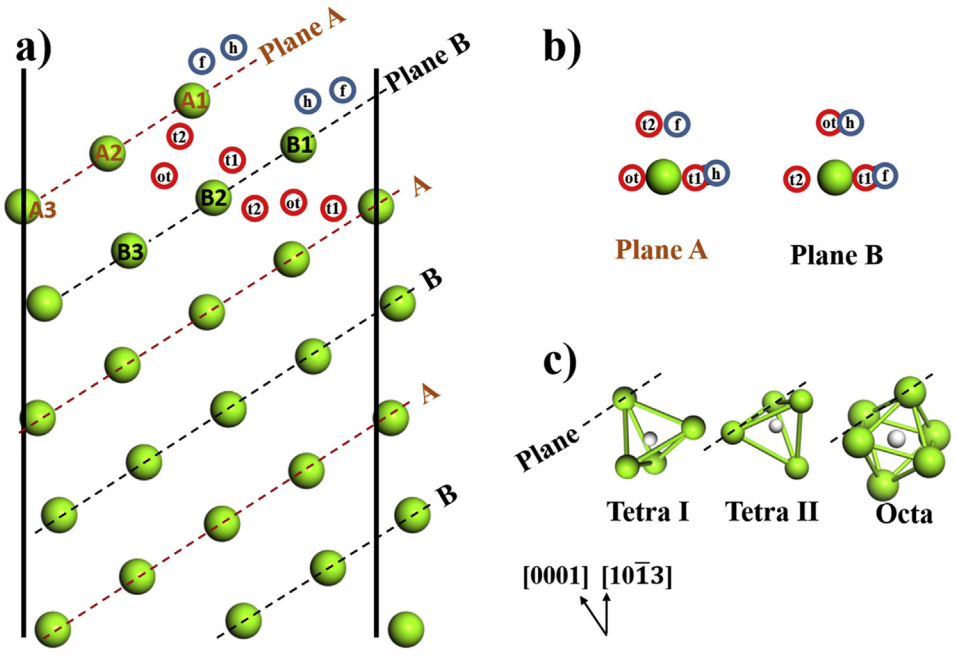

Fig. 1 – H adsorption sites on Mg(10$\bar{1}$3) surface: a) side view b) top view of Mg(10$\bar{1}$3) surface with adsorption sites (on-plane sites: fcc and hcp; sub-plane sites: tetra I, tetra II and octa) on Plane A and Plane B, and c) the illustration of the tetrahedral I, tetrahedral II and octahedral sub-plane sites. The blue sign in Fig. 1a) and b) represent the fcc and hcp on-plane hollow sites, respectively, while the red one indicates the sub-surface sites. (For interpretation of the references to colour in this figure legend, the reader is referred to the Web version of this article.)

Table 1 – Adsorption energy and Bader Charge of the first hydrogen on the fcc/hcp hollow sites on the outermost three Mg(10$\bar{1}$3) layers.

Adsorption site	Adsorption energy (eV/H)						Bader Charge for H (*e*)					
	A_1	A_2	A_3	B_1	B_2	B_3	A_1	A_2	A_3	B_1	B_2	B_3
fcc	−0.132	0.002	0.114	-[a]	-[a]	0.177	1.836	1.967	2.083	-[a]	-[a]	2.251
hcp	-[a]	−0.033	0.040	−0.081	-[a]	0.098	-[a]	1.983	1.985	1.955	-[a]	2.213

[a] - The hydrogen adsorption is not stable at the given site, and H moves to the adjacent stable site.

Table 2 – H adsorption energy on different adsorption site on Mg(0001) and Mg(10$\bar{1}$3).

Mg(0001)		Mg(10$\bar{1}$3)	
adsorption site	adsorption energy (eV/H)	adsorption site	adsorption energy (eV/H)
fcc	−0.071	A_1-fcc	−0.122
fcc [35]	−0.066	A_1-tetra I	0.122
fcc [23]	−0.05	A_2-hcp	−0.043
fcc [29]	−0.013	A_2-tetra I	0.098
fcc [30]	−0.005	A_2-tetra II	0.037
octa	0.218	A_3-hcp	0.045
octa [30]	0.27		

adsorbed at B_1-hcp and B_2-hcp sites, followed by the sequential adsorption of H on the B_1-hcp site forming H–Mg–H trilayer. From the configuration perspective, the fcc and tetra II hollow sites on Plane A are similar to the hcp and octa hollow sites on Plane B, where Mg locates in the middle of two H adsorption sites as shown in Fig. 1a. More specifically, the trilayer formation of H (A-fcc)–Mg (A)–H (A-tetra II) on Plane A is comparable to that of H (B-hcp)–Mg (B)–H (octa) on Plane B.

The adsorption sequences and average adsorption energies of Mg(10$\bar{1}$3) surface and Mg(0001) surface are compared, where hydrogen adsorption order of Mg(0001) surface is referred to previous studies [23]. As shown in Fig. 3, on the Mg(0001), the sequence of H adsorption are fcc, tetra II, octa and tetra II (of the second Mg layer) hollow sites. For the adsorption on Mg(10$\bar{1}$3), H is situated at fcc and tetra II sites at Plane A and hcp and octa sites at Plane B. There is a clear trend of H–Mg–H trilayer formation on both Mg(0001) surface and Mg(10$\bar{1}$3) surface, demonstrating that H–Mg–H trilayer is the stable structure, exhibiting the lowest E_{ad} among various structures, during initial H uptake. It is also shown that the initial H uptake on Mg(10$\bar{1}$3) from $\theta = 0.25$ ML to $\theta = 1$ ML and from $\theta = 2$ ML to $\theta = 3.25$ ML is much more energetically favorable than that on Mg(0001). For other coverage, Mg(0001) is slightly more advantageous. We will study the electron distribution and the hybridization in the following parts.

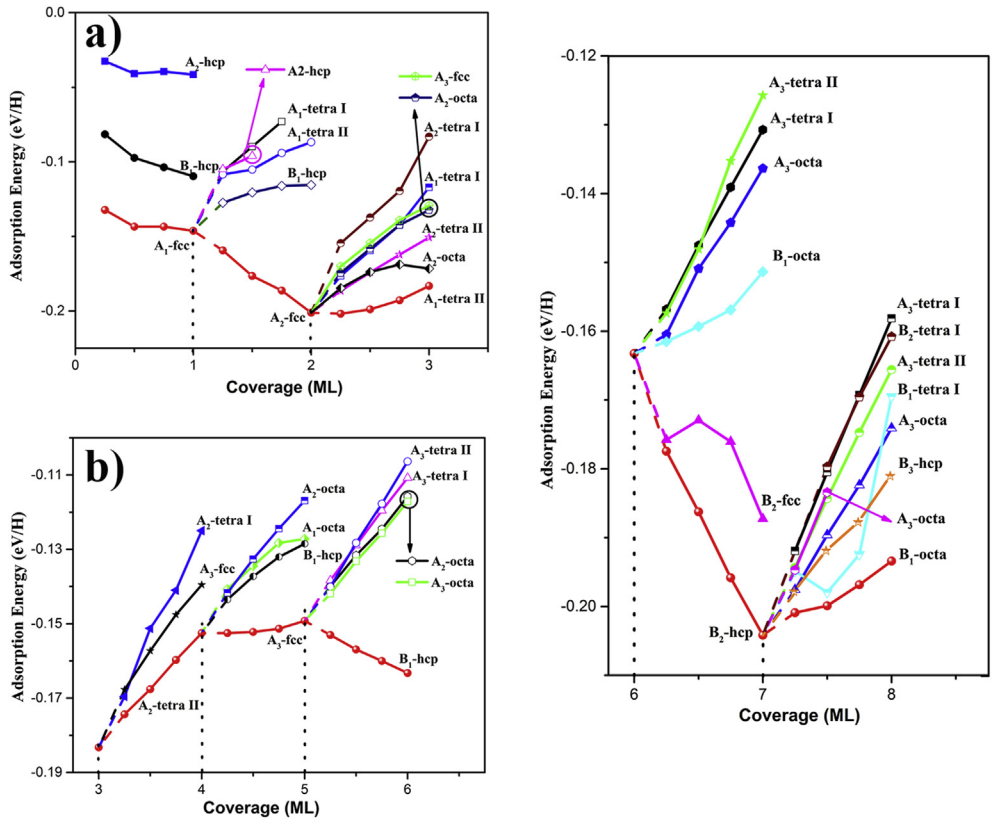

Fig. 2 – H adsorption energies from 1 ML to 9 ML on Mg(10$\bar{1}$3) surface. The conceivable adsorption sites are scrutinized based on the most thermodynamically stable H-adsorbed Mg system. The energetically advantageous adsorption sequence is: H (A_1-fcc), H (A_2-fcc), H (A_1-fcc), H (A_1-tetra II), H (A_2-tetra II), H (A_3-fcc), H (B_1-hcp), H (B_2-hcp) and H (B_1-octa).

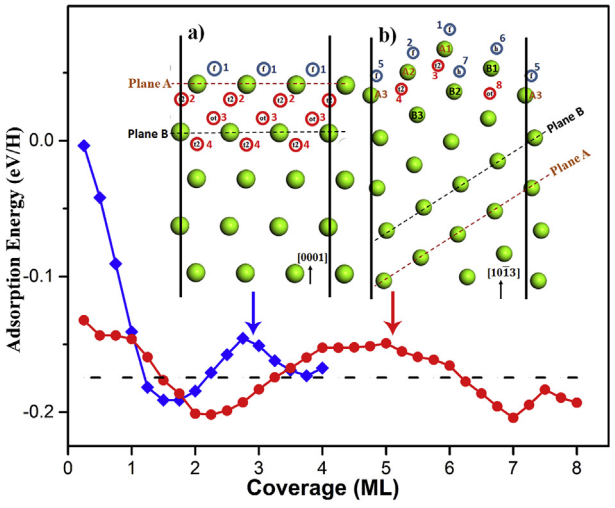

Fig. 3 – H adsorption energy (red circle and blue square points) and H uptake order on a) Mg(0001) surface and b) Mg(10$\bar{1}$3) surface. The dash line is the average adsorption energy (−1.75 eV/H) of hydrogen-adsorbed Mg(10$\bar{1}$3) surface from 1 ML to 8 ML. The blue curve and the red curve represent the average adsorption energies of H adsorbed Mg(0001) and Mg(10$\bar{1}$3). (For interpretation of the references to colour in this figure legend, the reader is referred to the Web version of this article.)

H adsorption mechanism on Mg(10$\bar{1}$3)

Previous literatures show that the "H–Mg–H trilayer" is a highly stable structure, where the middle Mg atom screens the electrostatic repulsion between two hydrogen atoms [23,32]. As shown in Fig. 3, although H adsorption on both high-index Mg(10$\bar{1}$3) and low-index Mg(0001) involves H–Mg–H trilayer, the H adsorption behaviors on Mg(10$\bar{1}$3) is very different from that on Mg(0001), including its unique adsorption sequence and the higher stability of adsorption under 1 ML. Therefore, it is reasonable to assume the H adsorption mechanism is changed on this high index surface. In details, the calculated projected density of states (PDOS) and Bader Charge analysis were employed to study the electron distribution and the hybridization of ideal H–Mg–H trilayer and H/Mg(0001) surface [48,49]. An ideal single H–Mg–H trilayer, where eight H atoms are located at the fcc/tetra II hollow sites of four Mg atoms, is modeled to evaluate the relaxed parameters as shown in Figure S1a. The PDOS in Figure S1b indicates that Mg 3*s* and 3*p* bands are mainly hybridized from the range of −3.0 eV to −0.5 eV, and overlap with H 1*s* band. The Mg–H bond lengths on each side are 2.040 Å and 2.042 Å with a bond angle of 179.8°. The Bader Charge analysis shows that Mg has 0.403 *e*, while two H atoms on different sides of Mg surface own 1.789 *e* and 1.808 *e*, respectively. Namely, each H has an electron gain of about 0.80 *e* and Mg has an electron loss of

about 1.60 *e*, indicating the formation of $Mg^{1.60+}$ and $H^{0.80-}$ ions in a highly stable H–Mg–H trilayer.

As H coverage increases from 0 ML to 4 ML over Mg(0001) in Fig. 3a, the adsorption energy dramatically drops to −0.201 eV/H then recovers to −0.153 eV/H. The average electron number of Mg located at the topmost layer decreases from 1.96 *e* to 0.40 *e*, while that of H adsorbed at the first three layers gradually approaches to be around 1.80 *e* (Table S9). The calculated results indicate that the Mg–H ionic bond forms, as reported previously [50,51]. On average, a transfer of approximately 0.13 *e* from H to Mg happens at $\theta = 1$ ML, while, interestingly, an inverse transfer of 0.79 *e* from Mg to H occurs, supporting that H–Mg–H trilayer with ionic Mg–H bond has formed. At the coverage of 4 ML, the bond lengths and bond angles of Mg(0001) are around 2.040 Å and 179.9°, respectively. The PDOS for clean and H-adsorbed Mg(0001) are shown in Figure S2. Mg 3*s* and 3*p* bands are hybridized and overlap with H 1*s* at $\theta > 0.25$ ML. The conformity in bond length and electron allocation of Mg(0001) and ideal H–Mg–H trilayer model indicates that H–Mg–H trilayer, which is weekly coupled to the substrates, can be a reliable indicator of stability [23]. We attempt to relate the bonding property and the charge configuration of $H^{0.80-}$ to the relative stabilities.

For the H uptake over the Mg(10$\bar{1}$3) surface, distortions are listed in Table S11. While H adsorb at A_1-fcc and B_1-hcp sites, the Mg–H bond lengths are around 1.886 Å and 1.890 Å, which are shorter than other bond lengths of the Mg(0001) surface or the ideal H–Mg–H model. The PDOS for Mg(10$\bar{1}$3) (Figure S3d ~ Figure S3h) reveals that Mg 3*s* and Mg 3*p* bands are hybridized when H is adsorbed. These details manifest that the H adsorption behavior is different on Mg(10$\bar{1}$3). According to the Bader Charge analyses listed in Table 1, a linear relation between charge allocation and adsorption energies of the first H adsorbed on Mg(10$\bar{1}$3) is depicted in Fig. 4. The more electron transfer to H atom, the higher adsorption energy is (i.e., the less stable the adsorption structure is). Thus, it is reasonable to deduce that the H charge of 1.80 *e* ($H^{0.80-}$) is a good criterion judging the stability of H adsorption structure on high-index surfaces. When H is adsorbed on Mg(10$\bar{1}$3), the electrons in surface dangling bonds can be transferred to H. H and Mg become charge negative and positive, respectively, forming Mg–H ionic bonds. However, the excessive electron of H atom could reduce the stabilization of the configuration.

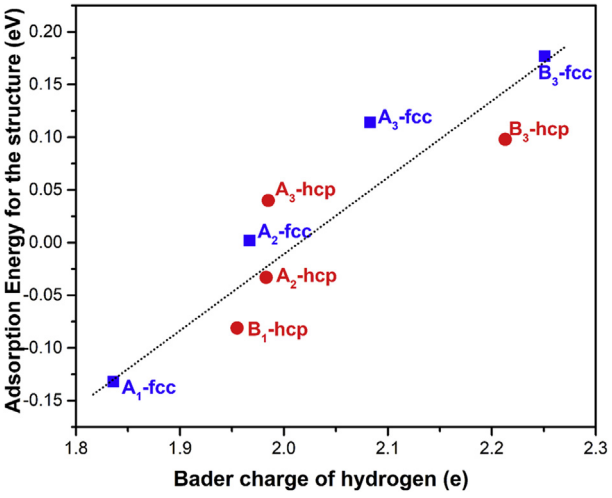

Fig. 4 – A linear relation between H charge and adsorption energies of the first H adsorbs on various sites on Mg(10$\bar{1}$3). The blue and red signs represent the H adsorb at fcc and hcp hollow sites, respectively. (For interpretation of the references to colour in this figure legend, the reader is referred to the Web version of this article.)

For the H uptake on Mg(10$\bar{1}$3), all structures and electron properties have been scrutinized to confirm the general applicability of the indicator of $H^{0.80-}$. Table 3 lists the Bader Charge of all the H adsorbed on Mg(10$\bar{1}$3). At the coverage of 1 ML, the most respective structures are H (A_1-fcc) and H (B_1-hcp) as depicted in Figure S3. The H (A_1-fcc) is slightly outward in the geometry then accepts less electrons (0.05 *e*) than H (B_1-hcp) from the surface, resulting that H (A_1-fcc) is more energetically favorable than H (B_1-hcp) by −0.036 eV/H. As the coverage increases to 2 ML, the configuration of H (A_1-fcc)/H (A_2-fcc) has the lowest adsorption energy of −0.201 eV/H and the lowest average H charge of 1.86 *e*/H, lower than 1.90 *e*/H and −0.115 eV/H of the H (A_1-fcc)/H (A_1-tetra II) configuration. The configurations of H (A_1-fcc)/H (A_1-tetra II) and H (A_1-fcc)/H (A_2-fcc) are compared in Figure S4. Theoretically, the configuration of H (A_1-fcc)/H (A_1-tetra II) forms a stable H–Mg–H trilayer. However, H (A_1-tetra II) bonds with Mg at different range with H (A_1-fcc) in PDOS (Figure S4g and S4h), indicating that it breaks Mg–Mg bond and serves as a "bridge" between Mg atoms. H (A_1-tetra II) accepts excessive electrons from adjacent Mg. When the coverage is more than 2 ML, the H adsorption energy is affected by complex factors, especially by Mg distortion. In the meanwhile, average Bader Charge converges to 1.80 *e*/H, demonstrating a trend toward H–Mg–H. Briefly, the charge on H is a reliable indicator for high-index Mg(10$\bar{1}$3) surface during initial H uptake, and H–Mg–H trilayer gradually forms as the coverage increases.

H_2 dissociation and H penetration on Mg(10$\bar{1}$3)

Our pervious study experimentally shows that Mg(10$\bar{1}$3) is a promising material that experimentally significantly reduces the H uptake temperature from 573 K to 392 K, and has a theoretical explanation of fast H diffusion along the closed-packed planes [16]. A complete hydrogen uptake of Mg material can be considered as several steps including H_2 dissociation, H penetration and possible phase transition, where the H_2 dissociation is the role step that requires high temperature [22–24,27]. During the reaction process, the slow hydrogen kinetics of H diffusion also dictates the need of high temperatures for hydrogen release [52,53]. The dissociation and diffusion are considered.

Fig. 5 shows the minimum energy path (MEP) of H_2 dissociation of Mg(0001) and Mg(10$\bar{1}$3). For H_2 dissociation on Mg(0001), the H molecule breaks into two H atoms separately located at fcc and hcp site, with an energy barrier of 0.85 eV consistent with 0.88 eV [25] and 0.85 eV [27] reported by Pozzo M and Alfè, and lower than 0.97 eV [35], 1.15 eV [26], 1.42 eV [24] eV and 1.38 [54] eV reported before. We indicate that the first H adsorbed on Mg(10$\bar{1}$3) is stable with an E_{ad} of −0.132 eV/H. In addition, since H preferentially adsorbs at A_1-fcc and A_2-fcc hollow sites on Mg(10$\bar{1}$3) during the initial H uptake, we

Table 3 – Bader Charge of H of the most stable adsorption configuration at various coverage on Mg(10$\bar{1}$3) surface.

Coverage (θ)	Average Bader Charges for hydrogen in the given location (*e*)								
	A_1-fcc	A_2-fcc	A_1-tetra II	A_2-tetra II	A_3-fcc	B_1-hcp	B_2-hcp	B_1-octa	average
1 ML	1.829	–	–	–	–	–	–	–	1.829
1 ML[*,a]	–	–	–	–	–	1.931	–	–	1.931
2 ML[*,b]	1.790	–	2.015	–	–	–	–	–	1.903
2 ML[*,c]	1.830	–	–	–	–	1.931	–	–	1.881
2 ML	1.805	1.906	–	–	–	–	–	–	1.856
3 ML	1.804	1.886	1.989	–	–	–	–	–	1.893
4 ML	1.778	1.811	1.927	2.051	–	–	–	–	1.892
5 ML	1.778	1.796	1.921	1.925	1.930	–	–	–	1.870
6 ML	1.774	1.797	1.917	1.905	1.876	1.862	–	–	1.855
7 ML	1.762	1.797	1.842	1.904	1.842	1.800	1.905	–	1.836
8 ML	1.762	1.798	1.845	1.943	1.850	1.767	1.859	1.878	1.838

[*] - The structure is not the most energetically favorable.
a, b, c and d -The H adsorb at: a, B_1-hcp; b, A_1-fcc/A_1-tetra II; c, A_1-fcc/A_1-tetra II hollow sites, respectively.

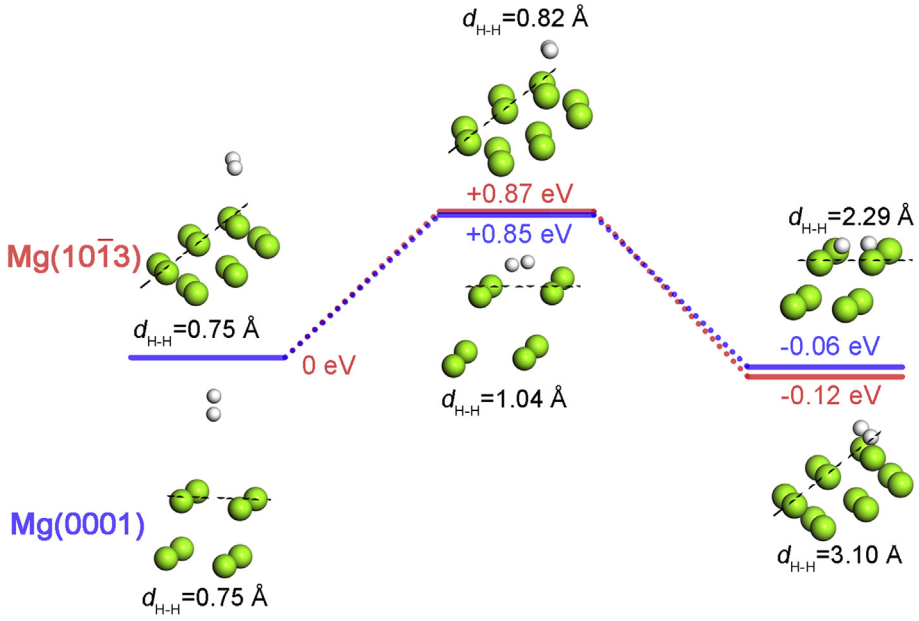

Fig. 5 – Minimum energy path barrier for H_2 dissociation on the Mg(10$\bar{1}$3) surface as compared to that on Mg(0001) surface.

focus on H_2 dissociation on Plane A as depicted in Figure S5. The MEP of Mg(10$\bar{1}$3) in Fig. 5 reveals that H_2 is more advantageous to dissociate at two A_1-fcc hollow sites with the energy barrier of 0.87 eV, close to that of Mg(0001). The calculation results show that H_2 dissociation energy barriers on Mg(10$\bar{1}$3) than on Mg(0001) are similar. The consequence on Mg(10$\bar{1}$3) is consistent with the adsorption sequence: H_2 firstly dissociate on A_1-fcc sites, then H diffuses to other stable sites.

For H diffusion on Mg(0001) and Mg(10$\bar{1}$3), H adsorption energies at each site are listed in Table 2. H diffusion from fcc to octa hollow site is the key step for H permeating into Mg(0001) as given in Fig. 6, and the penetration energy barrier is 0.48 eV, which is consistent with 0.45 eV reported by Wang, Zhang and co-workers [30,32], and lower than 0.69 eV [24] reported previously(more details of Mg(0001) comparison are listed in Table S12~S15). As given in Fig. 6, seven paths are designed taking A_1-fcc as inception point for Mg(10$\bar{1}$3). Path 1–4 and path 5–6 represent H diffusion along and penetrating the close-packed-plane, respectively. Intriguingly, we find that H migration from A_1-fcc to A_2-hcp (path 1) along Plane A is more energetically favored than to A_1-tetra I (path 5) penetrating Pane A by 0.21 eV, whereas H atom diffusion barrier from A_2-hcp to A_3-hcp (path 2) is 0.16 eV lower than that from A_2-hcp to A_2-tetra II (path 6). The profiles of energy barrier supports that H diffuses into Mg(10$\bar{1}$3) along the close-packed-planes [16]. Moreover, the role step of H diffusion into the bulk is escaping the A_1-fcc hollow site, at which H are located after H_2 facile dissociation.

The results imply that the role step of H uptake on Mg(0001) and Mg(10$\bar{1}$3) is H_2 dissociation, while their energy barriers are around 0.86 eV. The fabrication of Mg(10$\bar{1}$3) surface does not facilitate H_2 activation. Along with the H_2 dissociation, the challenge is to enable fast hydrogen kinetics (i.e., reduce diffusion energy barriers). H could only diffuse into the bulk by penetrating the closed-packed planes on Mg(0001), while it is available to diffuse both along the plane and through the

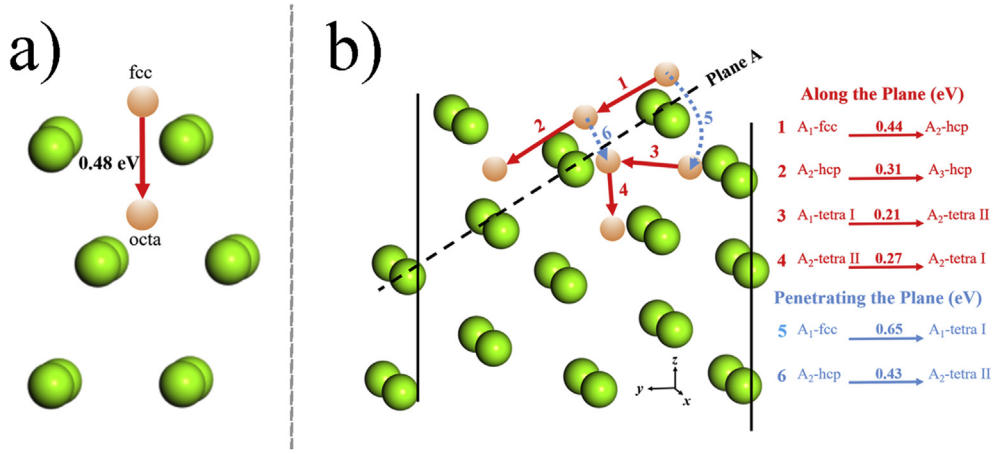

Fig. 6 – The pathways and energy barriers of H penetration on a) Mg(0001) from fcc to octa hollow site and b) Mg(10$\bar{1}$3).

planes on Mg(10$\bar{1}$3) as shown in Fig. 6. Moreover, the diffusion along the plane has a lower energy barrier than the one vertical to the plane. Consequently, a diffusion with lower energy barrier could be achieved on Mg(10$\bar{1}$3), which we assume can effectively weaken the "blocking effect" and lead to a decrease in experimental operation temperature. Briefly, the Mg(10$\bar{1}$3) has no advantage on H_2 dissociation while exhibits more H diffusion paths and a lower diffusion energy barrier than Mg(0001). This understanding of H sorption and kinetics facilitation of Mg(10$\bar{1}$3) can lead the design of Mg-based and other metal hydrogen storage materials to more accurately target the DOE goal of operating ambient temperature range from −40 °C to 60 °C with no allowable performance degradation from −20 °C to 40 °C [55].

Conclusion

Hydrogen adsorption is systematically studied on high-index Mg(10$\bar{1}$3) surface. Possible adsorption sites are considered and found to be in alignment with thoses on Mg(0001). The hydrogen adsorption sequence is: H (A_1-fcc), H (A_2-fcc), H (A_1-tetra II), H (A_2-tetra II), H (A_3-fcc), H (B_1-hcp), H (B_2-hcp) and H (B_1-octa), while all the adsorption sites are possible for hydrogen atoms to penetrate through the various orientations. The ideal electron allocations of $Mg^{1.60+}$ and $H^{0.80-}$ in H–Mg–H trilayer, a stable configuration in Mg(0001) surface as well as Mg(10$\bar{1}$3) surface, can be an indicator to evaluate the adsorption structure stability. The excessive electron over H atom could lower the H/Mg stability. For H initially adsorbed at Mg(10$\bar{1}$3) surface, a linear relationship is found between adsorption energy and allocated electron of hydrogen, and the distortion of Mg(10$\bar{1}$3) surface is primarily caused by the slight increase of interlayer spacing. Compared to Mg(0001) surface, where the Mg–H ionic bond that gradually strengthens as the coverage increases, Mg on Mg(10$\bar{1}$3) is more significantly coupled with H atoms since the first hydrogen atom. NEB results reveal that a better H kinetics performance on the high-index Mg(10$\bar{1}$3) surface. In details, H diffusion along the closed-packed-plane is more dynamically preferred on the high-index Mg(10$\bar{1}$3), manifested by the lower H diffusion energy barrier and the more diffusion paths, while Mg(10$\bar{1}$3) does not have advantage on H_2 dissociation. We attribute the decrease in experimental operation temperature to the diffusion advantages of the high-index surface rather than the dissociation one. This systematic study on the H adsorption sequence, mechanism, and the role step during H uptake on high-index Mg(10$\bar{1}$3) surface manifests the H sorption facilitation of this high-index surface. Besides, more property-impacting factors, such as strain, defect surfaces and transition metals doped surfaces, will be considered in our future studies, which can improve H sorption on Mg(0001) reported by Pozzo, Alfè, Du, Wang, Han, Lei and co-workers [24,28,29,34,36–38], for a better understanding of this high-index surface. Since the low-index and high-index surfaces widely exist in solid materials, the utilization of combination of low- and high-index surfaces also imply new possibilities for property improvements of various materials (e.g., solid fuel cell materials). We hope our study triggers more experimental and theoretical efforts to dig the potential of high-index surfaces.

Acknowledgments

This work is financially supported by NSFC (Grant Nos.11574088 and 51431001) and Major Science and Technology Projects of R & D and industrialization of key technologies for Maoming petrochemical industrial chain extension in Guangdong (2012A090300006). The computer times at National Supercomputing Center in Guangzhou (NSCCGZ) is gratefully acknowledged.

Appendix A. Supplementary data

Supplementary data to this article can be found online at https://doi.org/10.1016/j.ijhydene.2019.01.012.

REFERENCES

[1] Yang J, Sudik A, Wolverton C, Siegel DJ. High capacity hydrogen storage materials: attributes for automotive applications and techniques for materials discovery. Chem Soc Rev 2010;39:656–75. https://doi.org/10.1039/B802882F.

[2] Schlapbach L, Züttel A. Hydrogen-storage materials for mobile applications. Nature 2001;414:353–8. https://doi.org/10.1038/35104634.

[3] Raupach MR, Marland G, Ciais P, Le Quere C, Canadell JG, Klepper G, et al. Global and regional drivers of accelerating CO2 emissions. Proc Natl Acad Sci Unit States Am 2007;104:10288–93. https://doi.org/10.1073/pnas.0700609104.

[4] Jain IP, Lal C, Jain A. Hydrogen storage in Mg: a most promising material. Int J Hydrogen Energy 2010;35:5133–44. https://doi.org/10.1016/j.ijhydene.2009.08.088.

[5] Mao JF, Yu XB, Guo ZP, Liu HK, Wu Z, Ni J. Enhanced hydrogen storage performances of NaBH4-MgH2 system. J Alloy Comp 2009;479:619–23. https://doi.org/10.1016/j.jallcom.2009.01.012.

[6] Li Q, Li Y, Liu B, Lu X, Zhang T, Gu Q. The cycling stability of the in situ formed Mg-based nanocomposite catalyzed by YH_2. J Mater Chem 2017;5:17532–43. https://doi.org/10.1039/C7TA04551D.

[7] Xie L, Li J, Zhang T, Song L. Air-stable MgH 2 – CeO 2 composite with facilitated de/hydrogenation kinetics synthesized by high energy ball milling. Mater Char 2017;133:94–101. https://doi.org/10.1016/j.matchar.2017.09.031.

[8] Selvam P, Viswanathan B, Swamy CS, Srinivasan V. Magnesium and magnesium alloy hydrides. Int J Hydrogen Energy 1986;11:169–92. https://doi.org/10.1016/0360-3199(86)90082-0.

[9] Liang G, Huot J, Boily S, Van Neste a, Schulz R. Catalytic effect of transition metals on hydrogen sorption in nanocrystalline ball milled MgH2–Tm (Tm=Ti, V, Mn, Fe and Ni) systems. J Alloy Comp 1999;292:247–52. https://doi.org/10.1016/S0925-8388(99)00442-9.

[10] Rousselot S, Guay D, Roué L. Synthesis of fcc Mg-Ti-H alloys by high energy ball milling: structure and electrochemical hydrogen storage properties. J Power Sources 2010;195:4370–4. https://doi.org/10.1016/j.jpowsour.2009.12.138.

[11] Wang J, Wu F, Shan ZQ. Effect of addition of Mn and Co on the hydrogen storage characteristics of microcrystalline Mg. J Alloy Comp 2003;359:315–9. https://doi.org/10.1016/S0925-8388(03)00301-3.

[12] Ma M, Ouyang L, Liu J, Wang H, Shao H, Zhu M. Air-stable hydrogen generation materials and enhanced hydrolysis performance of MgH2-LiNH2composites. J Power Sources 2017;359:427–34. https://doi.org/10.1016/j.jpowsour.2017.05.087.

[13] Chen C, Wang J, Wang H, Liu T, Xu L, Li X. Improved kinetics of nanoparticle-decorated Mg-Ti-Zr nanocomposite for hydrogen storage at moderate temperatures. Mater Chem Phys 2018;206:21–8. https://doi.org/10.1016/j.matchemphys.2017.11.050.

[14] Zaluska A, Zaluski L, Ström-Olsen JO. Nanocrystalline magnesium for hydrogen storage. J Alloy Comp 1999;288:217–25. https://doi.org/10.1016/S0925-8388(99)00073-0.

[15] Sun Y, Shen C, Lai Q, Liu W, Wang DW, Aguey-Zinsou KF. Tailoring magnesium based materials for hydrogen storage through synthesis: current state of the art. Energy Storage Mater 2018;10:168–98. https://doi.org/10.1016/j.ensm.2017.01.010.

[16] Ouyang L, Tang J, Zhao Y, Wang H, Yao X, Liu J, et al. Express penetration of hydrogen on Mg(1013) along the close-packed-planes. Sci Rep 2015;5:1–9. https://doi.org/10.1038/srep10776.

[17] Hadjixenophontos E, Roussel M, Sato T, Weigel A, Stender P, Orimo S ichi, et al. Imaging the hydrogenation of Mg thin films. Int J Hydrogen Energy 2017;42:22411–6. https://doi.org/10.1016/j.ijhydene.2017.04.010.

[18] Tian M, Shang C. Mg-based composites for enhanced hydrogen storage performance. Int J Hydrogen Energy 2019;44:338–44.

[19] Tegner BE, Molinari M, Kerridge A, Parker SC, Kaltsoyannis N. Water adsorption on AnO2{111}, {110}, and {100} surfaces (An = U and Pu): a density functional theory + U study. J Phys Chem C 2017;121:1675–82. https://doi.org/10.1021/acs.jpcc.6b10986.

[20] Rák Z, Ewing RC, Becker U. Hydroxylation-induced surface stability of AnO2(An = U, Np, Pu) from first-principles. Surf Sci 2013;608:180–7. https://doi.org/10.1016/j.susc.2012.10.002.

[21] Liang Z, Li T, Kim M, Asthagiri A, Weaver JF. Low-temperature activation of methane on the IrO_2 (110) surface. Science 2017;356:299–303. https://doi.org/10.1126/science.aam9147.

[22] Tang JJ, Yang XB, Ouyang L, Zhu M, Zhao YJ. A systematic first-principles study of surface energies, surface relaxation and Friedel oscillation of magnesium surfaces. J Phys Appl Phys 2014;47. https://doi.org/10.1088/0022-3727/47/11/115305.

[23] Jiang T, Sun LX, Li WX. First-principles study of hydrogen absorption on Mg(0001) and formation of magnesium hydride. Phys Rev B Condens Matter 2010;81:1–9. https://doi.org/10.1103/PhysRevB.81.035416.

[24] Han Z, Chen H, Zhou S. Dissociation and diffusion of hydrogen on defect-free and vacancy defective Mg (0001) surfaces: a density functional theory study. Appl Surf Sci 2017;394:371–7. https://doi.org/10.1016/j.apsusc.2016.10.101.

[25] Pozzo M, Alfè D. Hydrogen dissociation on Mg(0001) studied via quantum Monte Carlo calculations. Phys Rev B Condens Matter 2008;78:1–5. https://doi.org/10.1103/PhysRevB.78.245313.

[26] Vegge T. Locating the rate-limiting step for the interaction of hydrogen with Mg(0001) using Density-Functional Theory calculations and rate theory. Phys Rev B Condens Matter 2004;70. https://doi.org/10.1103/PhysRevB.70.035412.

[27] Pozzo M, Alfè D. The role of steps in the dissociation of H2 on Mg(0001). J Phys Condens Matter 2009;21. https://doi.org/10.1088/0953-8984/21/9/095004.

[28] Pozzo M, Alfè D, Amieiro A, French S, Pratt A. Hydrogen dissociation and diffusion on Ni- and Ti-doped Mg(0001) surfaces. J Chem Phys 2008;128. https://doi.org/10.1063/1.2835541. 094703.

[29] Lei H, Wang C, Yao Y, Wang Y, Hupalo M, McDougall D, et al. Strain effect on the adsorption, diffusion, and molecular dissociation of hydrogen on Mg (0001) surface. J Chem Phys 2013;139. https://doi.org/10.1063/1.4839595.

[30] Xin J, Wang J, Du Y, Sun L, Huang B. Site preference and diffusion of hydrogen during hydrogenation of Mg: a first-principles study. Int J Hydrogen Energy 2016;41:3508–16. https://doi.org/10.1016/j.ijhydene.2015.12.157.

[31] Du AJ, Smith SC, Yao XD, Lu GQ. Catalytic effects of subsurface carbon in the chemisorption of hydrogen on a Mg(0001) surface: an ab-initio study. J Phys Chem B 2006;110:1814–9. https://doi.org/10.1021/jp055972d.

[32] Li Y, Zhang P, Sun B, Yang Y, Wei Y. Atomic hydrogen adsorption and incipient hydrogenation of the Mg(0001) surface: a density-functional theory study. J Chem Phys 2009;131. https://doi.org/10.1063/1.3182851. 034706.

[33] Uchida HT, Wagner S, Hamm M, Kürschner J, Kirchheim R, Hjörvarsson B, et al. Absorption kinetics and hydride formation in magnesium films: effect of driving force revisited. Acta Mater 2015;85:279–89. https://doi.org/10.1016/j.actamat.2014.11.031.
[34] Pozzo M, Alfè D. Hydrogen dissociation and diffusion on transition metal (= Ti, Zr, V, Fe, Ru, Co, Rh, Ni, Pd, Cu, Ag)-doped Mg(0001) surfaces. Int J Hydrogen Energy 2009;34:1922–30.
[35] Banerjee S, Pillai CGS, Majumder C. First-principles study of the H2 interaction with transition metal (Ti, V, Ni) doped Mg(0001) surface: implications for H-storage materials. J Chem Phys 2008;129:174703. https://doi.org/10.1063/1.3000673.
[36] Du AJ, Smith SC, Yao XD, Lu GQ. The role of Ti as a catalyst for the dissociation of hydrogen on a Mg(0001) surface. J Phys Chem B 2005;109:18037–41. https://doi.org/10.1021/jp052804c.
[37] Du AJ, Smith SC, Yao XD, Lu GQ. First-principle study of adsorption of hydrogen on Ti-doped Mg(0001) surface. J Phys Chem B 2006;110:21747–50. https://doi.org/10.1021/jp063286o.
[38] Du AJ, Smith SC, Yao XD, Lu GQ. Hydrogen spillover mechanism on a Pd-doped Mg surface as revealed by ab initio density functional calculation. J Am Chem Soc 2007;129:10201–4. https://doi.org/10.1021/ja0722776.
[39] Kresse G, Furthmüller J. Efficient iterative schemes for ab initio total-energy calculations using a plane-wave basis set. Phys Rev B Condens Matter 1996;54:11169–86. https://doi.org/10.1103/PhysRevB.54.11169.
[40] Joubert D. From ultrasoft pseudopotentials to the projector augmented-wave method. Phys Rev B Condens Matter 1999;59:1758–75. https://doi.org/10.1103/PhysRevB.59.1758.
[41] Kresse G, Hafner J. Ab initio molecular-dynamics simulation of the liquid-metalamorphous- semiconductor transition in germanium. Phys Rev B 1994;49:14251–69. https://doi.org/10.1103/PhysRevB.49.14251.
[42] Perdew J, Burke K, Ernzerhof M. Generalized gradient approximation made simple. Phys Rev Lett 1996;77:3865–8. https://doi.org/10.1103/PhysRevLett.77.3865.
[43] Chen M, Yang XB, Cui J, Tang JJ, Gan LY, Zhu M, et al. Stability of transition metals on Mg(0001) surfaces and their effects on hydrogen adsorption. Int J Hydrogen Energy 2012;37:309–17. https://doi.org/10.1016/j.ijhydene.2011.09.065.
[44] Swanson HE, Tatge E. Standard X-ray diffraction patterns. J Res Natl Bur Stand 1951;46:318. https://doi.org/10.6028/jres.046.036.
[45] Kittel C. Introduction to solid state physics. Solid State Phys 2005:703. https://doi.org/10.1119/1.1974177.
[46] Monkhorst HJ, Pack JD. Special points for Brillouin-zon integrations. Phys Rev B 1976;13:5188–92. https://doi.org/10.1103/PhysRevB.16.1748.
[47] Henkelman G, Jónsson H. Improved tangent estimate in the nudged elastic band method for finding minimum energy paths and saddle points. J Chem Phys 2000;113:9978–85. https://doi.org/10.1063/1.1323224.
[48] Henkelman G, Arnaldsson A, Jónsson H. A fast and robust algorithm for Bader decomposition of charge density. Comput Mater Sci 2006;36:354–60. https://doi.org/10.1016/j.commatsci.2005.04.010.
[49] Sanville E, Kenny SD, Smith R, Henkelman G. Improved grid-based algorithm for Bader charge allocation. J Comput Chem 2007;28:899–908. https://doi.org/10.1002/jcc.20575.
[50] Transactions ECS, Society TE. Understanding charge transfer at Mg/MgH2 interfaces for hydrogen storage 2017;77:81–90.
[51] Sun G, Li Y, Zhao X, Wu J, Wang L, Mi Y. First-principles investigation of the effects of Ni and Y co-doped on destabilized MgH_2. RSC Adv 2016;6:23110–6. https://doi.org/10.1039/C5RA23996F.
[52] Niemann MU, Srinivasan SS, Phani AR, Kumar A, Goswami DY, Stefanakos EK. Nanomaterials for hydrogen storage applications: a review. J Nanomater 2008;2008. https://doi.org/10.1155/2008/950967.
[53] Bérubé V, Radtke G, Dresselhaus M, Chen G. Size effects on the hydrogen storage properties of nanostructured metal hydrides: a review. Int J Energy Res 2007;31:637–63. https://doi.org/10.1002/er.1284.
[54] Jian Z, Dianwu Z, Yani H, Ping P, Jinshui L. Study on H2 adsorption and dissociation properties on Mg(0001) surface. Rare Metal Mater Eng 2009;38:1518–25. https://doi.org/10.1016/S1875-5372(10)60049-5.
[55] https://www.energy.gov/eere/fuelcells/doe-technical-targets-onboard-hydrogen-storage-light-duty-vehicles n.d..